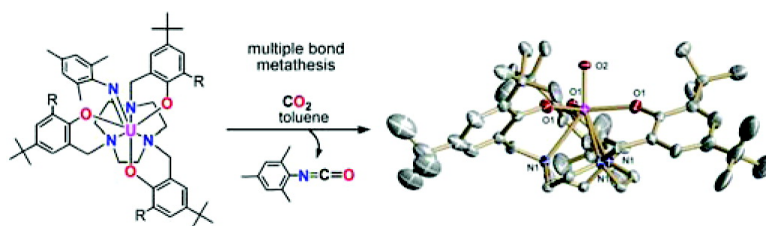


Carbon Dioxide Activation with Sterically Pressured Mid- and High-Valent Uranium Complexes

Suzanne C. Bart, Christian Anthon, Frank W. Heinemann, Eckhard Bill, Norman M. Edelstein, and Karsten Meyer

J. Am. Chem. Soc., **2008**, 130 (37), 12536-12546 • DOI: 10.1021/ja804263w • Publication Date (Web): 21 August 2008

Downloaded from <http://pubs.acs.org> on February 8, 2009



More About This Article

Additional resources and features associated with this article are available within the HTML version:

- Supporting Information
- Access to high resolution figures
- Links to articles and content related to this article
- Copyright permission to reproduce figures and/or text from this article

[View the Full Text HTML](#)



ACS Publications
 High quality. High impact.

Carbon Dioxide Activation with Sterically Pressured Mid- and High-Valent Uranium Complexes

Suzanne C. Bart,[†] Christian Anthon,[†] Frank W. Heinemann,[†] Eckhard Bill,[§]
Norman M. Edelstein,[‡] and Karsten Meyer^{*†}

University of Erlangen-Nürnberg, Department of Chemistry and Pharmacy, Inorganic Chemistry,
Egerlandstrasse 1, 91058 Erlangen, Germany, Chemical Sciences Division, MS70A-1150,
Lawrence Berkeley National Laboratory, Berkeley, California 94720-8175, and Max-Planck
Institute for Bioinorganic Chemistry, Stiftstrasse 34-36,
D-45470, Mülheim an der Ruhr, Germany

Received June 14, 2008; E-mail: kmeyer@chemie.uni-erlangen.de

Abstract: Sterically pressured mid- to high-valent uranium complexes with an aryloxy substituted triazacyclononane ligand scaffold, $[(^R\text{ArO})_3\text{taccn}]^{3-}$, were studied for carbon dioxide activation and transformation chemistry. The high valent uranium(V) imido species $[(^R\text{ArO})_3\text{taccn}]\text{U}(\text{NR})$ (R = ^tBu, R' = 2,4,6-trimethylphenyl (**2-^tBu**); R = Ad, R' = 2,4,6-trimethylphenyl (**2-Ad**); R = ^tBu, R' = phenyl (**3-^tBu**)) were synthesized and spectroscopically characterized. X-ray crystallography of the *tert*-butyl mesityl imido derivative, **2-^tBu**, reveals coordination of a bent imido fragment with a relatively long U–N bond distance of 2.05 Å. The mesityl imido complexes reacted with carbon dioxide, readily extruding free isocyanate to produce uranium(V) terminal oxo species, $[(^R\text{ArO})_3\text{taccn}]\text{U}(\text{O})$ (R = ^tBu (**4-^tBu**), Ad (**4-Ad**)), presumably through multiple bond metathesis via a uranium(V) carbamate intermediate. Using the smaller phenyl imido fragment in **3-^tBu** slowed isocyanate loss, allowing the uranium(V) carbamate intermediate to undergo a second metathesis reaction, ultimately producing the diphenyl ureate derivative, $[(^R\text{ArO})_3\text{taccn}]\text{U}(\text{NPh}_2)\text{CO}$ (**5-^tBu**). Single crystal X-ray diffraction studies were carried out on both uranium(V) terminal oxo complexes and revealed short U–O bonds (1.85 Å) indicative of a formal U=O triple bond. The electronic structure of the oxo U(V) complexes was investigated by electronic absorption and EPR spectroscopies as well as SQUID magnetization and DFT studies, which indicated that their electronic properties are highly unusual. To obtain insight into the reactivity of CO₂ with U–N bonds, the reaction of the uranium(IV) amide species, $[(^R\text{ArO})_3\text{taccn}]\text{U}(\text{NHMe})$ (R = ^tBu (**6-^tBu**), Ad (**6-Ad**)) with carbon dioxide was investigated. These reactions produced the uranium(IV) carbamate complexes, $[(^R\text{ArO})_3\text{taccn}]\text{U}(\text{CO}_2\text{NHMe})$ (R = ^tBu (**7-^tBu**), Ad (**7-Ad**)), resulting from insertion of carbon dioxide into U–N(amide) bonds. The molecular structures of the synthesized uranium carbamate complexes highlight the different reactivities due to the steric pressure introduced by the alkyl derivatized tris(aryloxy) triazacyclononane ligand. The sterically open *tert*-butyl derivative creates a monodentate η¹-O bound carbamate species, while the sterically more bulky adamantyl-substituted compound forces a bidentate κ²-O,O coordination mode of the carbamate ligand.

Introduction

Small carbon containing molecules such as methane, carbon monoxide, and carbon dioxide are attractive chemical feedstocks as they are inexpensive and readily available.^{1–3} To activate these small, inert molecules, a potent electron source is needed to reduce their thermodynamically stable bonds.^{4,5} Transition metal catalysts coupled with reducing agents have proven effective for reducing carbon dioxide, and a variety of trans-

formations have resulted in activation and incorporation of CO₂ into larger molecules to obtain the functionalized products.^{4,6–8} Low-valent f-block elements are especially attractive prospects for carbon dioxide reduction and activation because they are highly reducing oxophilic metals that can mediate one-electron and multielectron redox processes.

One of the first indications that carbon dioxide could be activated by uranium was reported in the mid 1980s, with the activation of the carbon dioxide analogue, carbonyl sulfide, SCO.⁹ Exposure of the trivalent uranium metallocene, $[(\eta^5\text{-C}_5\text{H}_4\text{Me})_3\text{U}(\text{THF})]$ to an excess of SCO resulted in a two-electron reduction of the small molecule to produce the bridging

[†] University of Erlangen-Nürnberg.

[§] Max-Planck Institute of Bioinorganic Chemistry.

[‡] Lawrence Berkeley National Laboratory.

(1) Olah, G. A.; Goepfert, A.; Prakash, S. G. K. *Beyond Oil and Gas: The Methanol Economy*; Wiley-VCH: Weinheim, Germany, 2006.

(2) Tolman, W. B. *Activation of Small Molecules*; Wiley-VCH; Weinheim, Germany, 2006.

(3) Aresta, M.; Dibenedetto, A. *Dalton Trans.* **2007**, 2975.

(4) Lee, C. H.; Laitar, D. S.; Mueller, P.; Sadighi, J. P. *J. Am. Chem. Soc.* **2007**, *129*, 13802.

(5) Castro-Rodriguez, I.; Meyer, K. *J. Am. Chem. Soc.* **2005**, *127*, 11242–11243.

(6) Louie, J.; Gibby, J. E.; Farnworth, M. V.; Tekavec, T. N. *J. Am. Chem. Soc.* **2002**, *124*, 15188.

(7) Takimoto, M.; Mori, M. *J. Am. Chem. Soc.* **2002**, *124*, 10008.

(8) Sadique, A. R.; Brennessel, W. W.; Holland, P. L. *Inorg. Chem.* **2008**, *47*, 784.

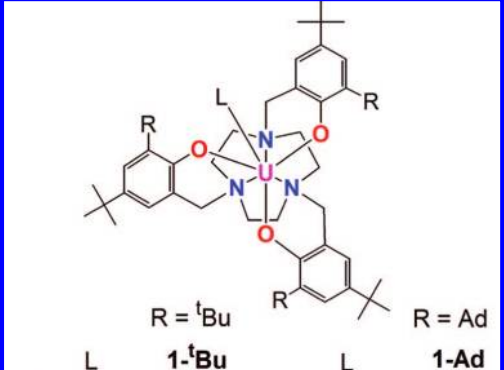
(9) Brennan, J. G.; Andersen, R. A.; Zalkin, A. *Inorg. Chem.* **1986**, *25*, 1761–1765.

sulfido species, $[(\eta^5\text{-C}_5\text{H}_4\text{Me})_3\text{U}]_2(\mu\text{-S})$, with concomitant loss of carbon monoxide. Following this report of SCO activation, similar reduction of carbon dioxide was later observed with low valent uranium complexes supported by a macrocyclic polyamine chelator. The *tert*-butyl-derivatized aryloxy-functionalized triazacyclononane uranium(III) complex, $[(\text{}^t\text{BuArO})_3\text{tacn}]\text{U}$, reduces carbon dioxide by two electrons (one from each uranium) to release carbon monoxide and produce a dinuclear U(IV/IV) bridging μ -oxo species, $[(\text{}^t\text{BuArO})_3\text{tacn}]_2\text{U}_2(\mu\text{-O})$.⁵ Exchanging the ortho *tert*-butyl substituent on the aryloxy ligands for adamantyl groups to form $[(\text{}^{\text{Ad}}\text{ArO})_3\text{tacn}]\text{U}$ (**1-Ad**) changes the reactivity with CO₂. Addition of carbon dioxide gas to the sterically more demanding adamantyl functionalized complex **1-Ad** produces a previously unknown η^1 -OCO uranium complex, $[(\text{}^{\text{Ad}}\text{ArO})_3\text{tacn}]\text{U}(\eta^1\text{-OCO})$, where the carbon dioxide ligand is bound η^1 end-on through one of the oxygen atoms.¹⁰ The carbon dioxide fragment in this molecule is partially reduced, and the complex can be formulated as a radical anionic species, U(IV)-L⁻, as confirmed by crystallographic, magnetic, and spectroscopic (IR, UV/vis/NIR, and XANES) analysis. The carbon dioxide ligand is protected from further reduction by low-valent uranium starting material in solution, because the adamantyl groups encapsulate the uranium and eliminate complications from decomposition and dimerization pathways.

Several examples of carbon dioxide functionalization by f-block systems have also been described. Evans reported that the addition of carbon dioxide to $[(\text{C}_5\text{Me}_5)_2\text{Sm}(\text{THF})_2]$ resulted in reductive dimerization of CO₂ to produce the oxalate complex, $[(\text{C}_5\text{Me}_5)_2\text{Sm}]_2(\mu\text{-}\eta^2\text{:}\eta^2\text{-O}_2\text{CCO}_2)$.¹¹ It is proposed that the samarium center initially coordinates and reduces the CO₂ fragment to generate a radical species, $[\text{CO}_2]^-$, which then immediately couples with another equivalent to generate the observed dimer. Later, the same group demonstrated that addition of carbon dioxide to a family of trivalent metallocene complexes $[(\eta^5\text{-C}_5\text{Me}_4\text{H})_3\text{M}]$ (M = La, Ce, Pr, Nd, Sm) resulted in insertion of CO₂ into one of the M–C bonds of the coordinated Cp derivative to form $\{[(\eta^5\text{-C}_5\text{Me}_4\text{H})_2\text{M}](\mu\text{-}\eta^1\text{:}\eta^1\text{-O}_2\text{CC}_5\text{Me}_4\text{H})\}_2$.¹² Insertion of CO₂ into Sm–S and Sm–Se bonds of $[(\eta^5\text{-C}_5\text{Me}_5)_2\text{Sm}(\mu\text{-EPh})_2]$ (E = S, Se) generated the first crystallographically characterized complexes featuring an $(\text{O}_2\text{CEPh})^{1-}$ ligand, namely $[(\eta^5\text{-C}_5\text{Me}_5)_2\text{Sm}(\mu\text{-O}_2\text{CEPh})_2]$.¹³ Similar instances of carbon dioxide insertion into uranium chalcogenide bonds have been observed for the reaction of the uranium(IV) dithiolate complex $[(\eta^5\text{-C}_5\text{Me}_5)_2\text{U}(\text{S}^t\text{Bu})_2]$ with CO₂, affording the insertion product $[(\eta^5\text{-C}_5\text{Me}_5)_2\text{U}(\text{O}_2\text{-CS}^t\text{Bu})_2]$.¹⁴ Thermolysis of this complex resulted in extrusion of the carbon dioxide.

To determine if similar activation and functionalization of carbon dioxide could be achieved with the previously discussed aryloxy-substituted triazacyclononane uranium complexes, mid- and high valent uranium amido and imido derivatives, U–NHR and U=NR, were prepared and explored. Herein, we report the synthesis and characterization of the complexes resulting from carbon dioxide activation by X-ray crystallography and IR vibrational, electronic absorption, and EPR

Chart 1. Table of Compounds



R = ^t Bu		R = Ad	
L	1- ^t Bu	L	1-Ad
(=NMe _s)	2- ^t Bu	(=NMe _s)	2-Ad
(=NPh)	3- ^t Bu		
(=O)	4- ^t Bu	(=O)	4-Ad
((NPh) ₂ CO)	5- ^t Bu		
(-NHMe _s)	6- ^t Bu	(-NHMe _s)	6-Ad
(-CO ₂ NHMe _s)	7- ^t Bu	(-CO ₂ NHMe _s)	7-Ad

spectroscopies, as well as SQUID magnetization studies and DFT calculations (Chart 1).

Results and Discussion

Synthesis and Characterization of Uranium(V) Complexes.

Addition of mesityl azide to red brown pentane solutions of the two uranium(III) complexes, $[(\text{}^{\text{R}}\text{ArO})_3\text{tacn}]\text{U}$ (R = ^tBu (**1-^tBu**), Ad (**1-Ad**))^{15,16} causes immediate evolution of dinitrogen consistent with the formation of the imido species as well as simultaneous precipitation of a dark brown solid, assigned as $[(\text{}^{\text{R}}\text{ArO})_3\text{tacn}]\text{U}(\text{NMe}_s)$ (R = ^tBu (**2-^tBu**), Ad (**2-Ad**)) (Scheme 1), isolable by vacuum filtration.

Cooling a concentrated pentane/ether (7:3) solution to –35 °C produced X-ray quality crystals of $[(\text{}^{\text{t}}\text{BuArO})_3\text{tacn}]\text{U}(\text{NMe}_s)$ (**2-^tBu**). The uranium(V) imido complex **2-Ad** was fully characterized; however, crystals suitable for an X-ray diffraction analysis were not obtained. The molecular structure of the *tert*-butyl derivative **2-^tBu** shows a seven coordinate uranium atom with an axially bound bent imido ligand (Figure 1). The respective U–O(ArO)_{av} and the U–N(tacn)_{av} bond distances of 2.19 and 2.72 Å as well as the displacement of the uranium center 0.166(4) Å below the trigonal plane of the three aryloxy oxygen atoms are within the expected range for U(V) imido complexes of the $(\text{}^{\text{R}}\text{ArO})_3\text{tacn}^{3-}$ ligand set.¹⁷ The U–N(imido) bond length of 2.047(8) Å is similar to those previously reported for U(V) and U(VI) imido complexes of other ligand systems,^{18–21} which have U–N(imido) distances ranging from 1.90 to 2.12 Å. This U–N(imido) bond length of **2-^tBu** is slightly

(10) Castro-Rodríguez, I.; Nakai, H.; Zakharov, L. N.; Rheingold, A. L.; Meyer, K. *Science* **2004**, *305*, 1757–1760.

(11) Evans, W. J.; Seibel, C. A.; Ziller, J. W. *Inorg. Chem.* **1998**, *37*, 770–776.

(12) Evans, W. J.; Rego, D. B.; Ziller, J. W.; DiPasquale, A. G.; Rheingold, A. L. *Organometallics* **2007**, *26*, 4737–4745.

(13) Evans, W. J.; Miller, K. A.; Ziller, J. W. *Inorg. Chem.* **2006**, *45*, 424–429.

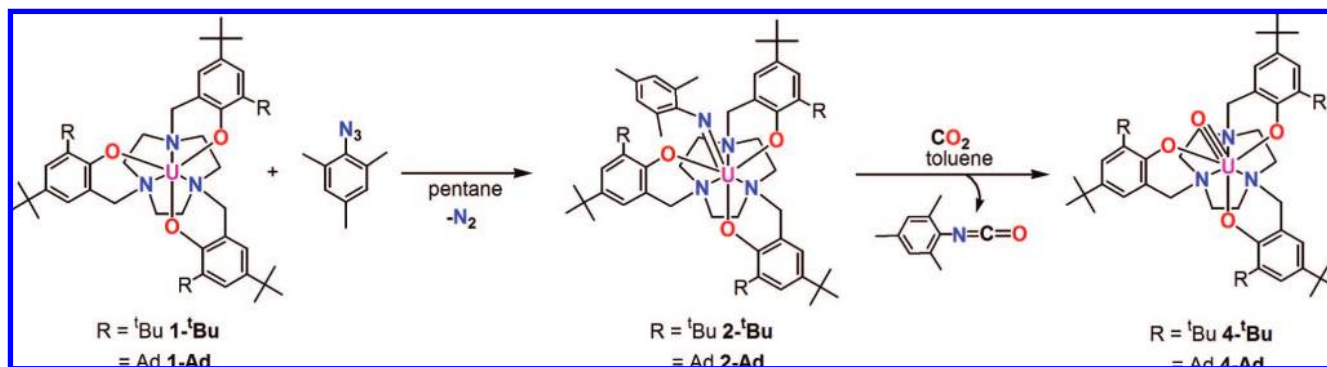
(14) Lescop, C.; Arliguie, T.; Lance, M.; Nierlich, M.; Ephritikhine, M. *J. Organomet. Chem.* **1999**, *580*, 137–144.

(15) Nakai, H.; Hu, X.; Zakharov, L. N.; Rheingold, A. L.; Meyer, K. *Inorg. Chem.* **2004**, *43*, 855–857.

(16) Castro-Rodríguez, I.; Olsen, K.; Gantzel, P.; Meyer, K. *J. Am. Chem. Soc.* **2003**, *125*, 4565–4571.

(17) Castro-Rodríguez, I.; Meyer, K. *Chem. Commun.* **2006**, 1353–1368.

Scheme 1. Synthesis of Uranium(V) Imido Complexes, $[(^R\text{ArO})_3\text{tacn}]\text{U}(\text{NMes})$ ($R = {}^t\text{Bu}$ (**2-*t*Bu**); Ad (**2-Ad**)), and Uranium(V) Oxo Complexes, $[(^R\text{ArO})_3\text{tacn}]\text{U}(\text{O})$ ($R = {}^t\text{Bu}$ (**4-*t*Bu**); Ad (**4-Ad**))



longer than that of the previously synthesized uranium(V) trimethylsilyl imido complex, $[(^{\text{tBu}}\text{ArO})_3\text{tacn}]\text{U}(\text{NSiMe}_3)$, which features a U–N bond length of 1.989(5) Å.^{16,22} The most notable structural difference between this known compound and newly synthesized **2-*t*Bu** is the angle of the U–N–C_{Ar} imido fragment. The U–N–C angle of **2-*t*Bu** is bent at 154.7(8)°, while the angle for $[(^{\text{tBu}}\text{ArO})_3\text{tacn}]\text{U}(\text{NSiMe}_3)$ is close to linear with a U–N–Si angle of 173.7(3)°. This can be attributed to steric and electronic differences between the two imido fragments (alkyl/silyl vs aryl).²³ The trimethylsilyl group is cylindrical, and fits nicely in the cavity created by the *tert*-butyl substituents on the $(^{\text{tBu}}\text{ArO})_3\text{tacn}^{3-}$ ligand, allowing for optimal binding to the uranium center and formation of one formal σ and two degenerate π bonds. Coordination of the more bulky ortho-methylated mesityl imido ligand of **2-*t*Bu**, on the other hand, is sterically hindered by interference with the *tert*-butyl groups of the $(^{\text{tBu}}\text{ArO})_3\text{tacn}^{3-}$ chelator. This steric constraint prevents optimal overlap with the uranium atom's π -orbitals leading to the slightly bent structure, where the methyl groups on the imido fragment are tucked into the clefts formed by the *tert*-butyl groups (see Supporting Information, Figure S1).

The bent structure observed for **2-*t*Bu** closely resembles that of the previously reported adamantyl functionalized uranium trimethylsilyl imido complex, $[(^{\text{Ad}}\text{ArO})_3\text{tacn}]\text{U}(\text{NSiMe}_3)$, which features a slightly longer U–N bond length of 2.122(2) Å and a similarly bent imido ligand with a U–N–Si angle of 162.6(2)°. In this case, the bent imido fragment also is reactive and undergoes multiple bond metathesis with π -acids, such as carbon monoxide and methyl isocyanide, to produce the corresponding U(IV) isocyanate and carbodiimide compounds.²⁴ In contrast, the linear imido ligand of the corresponding *tert*-butyl derivative, $[(^{\text{tBu}}\text{ArO})_3\text{tacn}]\text{U}(\text{NSiMe}_3)$, is unreactive toward these π acids. The increased reactivity of the adamantyl derivatized trimethylsilyl imido complex is attributed to the bent structure of the imido species, which—similar to **2-*t*Bu**—results from increased steric pressure in the system. As a result of the inferior M–L bonding and as a consequence the longer U–N

bond distance, the nucleophilic character on the imido nitrogen of this compound appears to be enhanced, thus allowing attack of π acids. Since the bending of the imido fragment of **2-*t*Bu** is similar to $[(^{\text{Ad}}\text{ArO})_3\text{tacn}]\text{U}(\text{NSiMe}_3)$, it appears reasonable that this complex is similarly reactive toward small molecules.

To test this hypothesis, toluene solutions of both dark brown uranium(V) mesityl imido species **2-*t*Bu** and **2-Ad** were stirred under an atmosphere of CO₂ (Scheme 1). Both imido derivatives, $[(^R\text{ArO})_3\text{tacn}]\text{U}=\text{NMes}$, produced bright orange slurries within minutes of vigorous stirring. Removal of the solvent in vacuo followed by IR analysis of the crude material revealed a band at 2286 cm⁻¹ (nujol), consistent with formation of free mesityl isocyanate (solid, MP = 44 °C). This side product was easily removed by washing the resulting orange residue thoroughly with pentane.

Analysis of single crystals by X-ray diffraction revealed the formation of terminal oxo species of the form $[(^R\text{ArO})_3\text{tacn}]\text{U}(\text{O})$ ($R = {}^t\text{Bu}$ (**4-*t*Bu**); Ad (**4-Ad**)) (Figure 2, metrical parameters in Table 1). In the molecular structure of **4-*t*Bu**, the U–O(oxo) bond lies on a crystallographic 3-fold symmetry axis, rendering all uranium $(^R\text{ArO})_3\text{tacn}^{3-}$ ligand N/O distances equivalent. The respective U–O(ArO) and the U–N(tacn) bond lengths of 2.203(5) and 2.677(7) Å for **4-*t*Bu** are similar to those for the uranium(V) imido species **2-*t*Bu**. For **4-Ad**, the 3-fold axis is absent, but the respective U–O(ArO)_{av} and U–N(tacn)_{av} ligand bond distances of 2.18 and 2.73 Å are within the expected range. For **4-*t*Bu** and **4-Ad**, the respective uranium terminal oxo bond distances, $d(\text{U}=\text{O})$, of 1.848(8) Å (**4-*t*Bu**) and 1.848(4) Å (**4-Ad**) are similar to the distance of 1.859(6) Å observed for

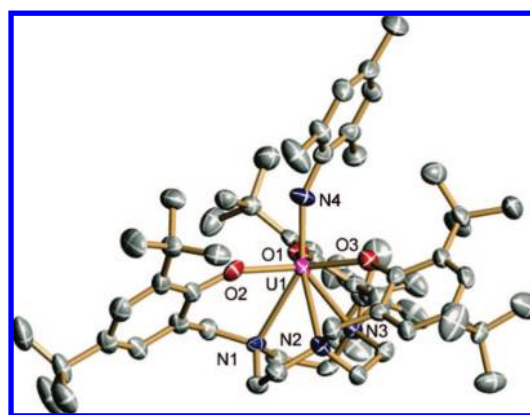


Figure 1. Molecular structure of $[(^{\text{tBu}}\text{ArO})_3\text{tacn}]\text{U}(\text{NMes})$ (**2-*t*Bu**) in crystals of **2-*t*Bu**·*n*-C₅H₁₂ shown with 50% probability ellipsoids. Hydrogen atoms and solvent molecules omitted for clarity.

- (18) Kiplinger, J. L.; Morris, D. E.; Scott, B. L.; Burns, C. J. *Organometallics* **2002**, *21*, 3073–3075.
- (19) Arney, D. S. J.; Burns, C. J. *J. Am. Chem. Soc.* **1995**, *117*, 9448–60.
- (20) Warner, B. P.; Scott, B. L.; Burns, C. J. *Angew. Chem., Int. Ed.* **1998**, *37*, 959–960.
- (21) Zalkin, A.; Brennan, J. G.; Andersen, R. A. *Acta Crystallogr., Sect. C* **1988**, *C44*, 1553–1554.
- (22) Average of two independent molecules in the unit cell.
- (23) Hrovat, D. A.; Waali, E. E.; Borden, W. T. *J. Am. Chem. Soc.* **1992**, *114*, 8698–8699.
- (24) Castro-Rodriguez, I.; Nakai, H.; Meyer, K. *Angew. Chem., Int. Ed.* **2006**, *45*, 2389–2392.

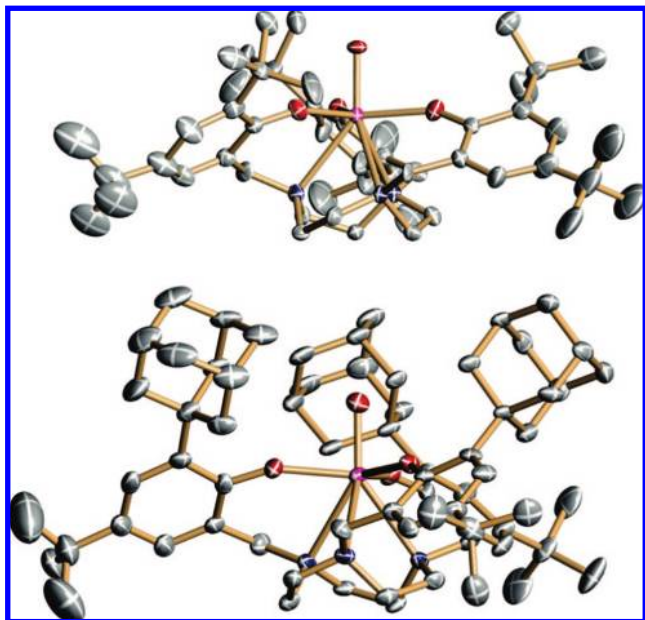


Figure 2. Molecular structures of $[(^t\text{BuArO})_3\text{tacn}]\text{U}(\text{O})$ (**4-Bu**) in crystals of **4-Bu**· $3n\text{-C}_5\text{H}_{12}$ (top) and $[(^{\text{Ad}}\text{ArO})_3\text{tacn}]\text{U}(\text{O})$ (**4-Ad**) in crystals of **4-Ad**· $1.5\text{C}_6\text{H}_5\text{Me}\cdot 0.5n\text{-C}_5\text{H}_{12}$ (bottom) shown with 50% probability ellipsoids. Hydrogen atoms and solvent molecules are omitted for clarity.

Table 1. Selected Distances (Å) and Angles (deg) for the Uranium(V) Complexes

structural parameters	2- ^t Bu	4- ^t Bu	4-Ad	5- ^t Bu
U–N ₁ _{tacn}	2.765(8)	2.677(7)	2.705(5)	2.788(4)
U–N ₂ _{tacn}	2.699(9)	2.677(7)	2.736(5)	2.796(4)
U–N ₃ _{tacn}	2.690(7)	2.677(7)	2.754(5)	2.684(4)
U–N _{av}	2.72	2.677(7)	2.73	2.76
U–O ₁ _{ArO}	2.194(7)	2.203(5)	2.186(4)	2.161(3)
U–O ₂ _{ArO}	2.160(6)	2.203(5)	2.170(4)	2.114(3)
U–O ₃ _{ArO}	2.205(7)	2.203(5)	2.180(4)	2.149(3)
U–O _{av}	2.19	2.203(5)	2.18	2.14
U–N _{imido}	2.047(8)			
U–N–C _{imido}	154.7(8)			
U–O _{oxo}		1.848(8)	1.848(4)	
U–N _{ureate}				2.329(4), 2.310(4)
U _{out-of-plane shift}	0.166(4)	0.165(9)	0.147(3)	0.286(2)

the only other crystallographically characterized monomeric uranium(V) terminal oxo species, $[(\text{Cp}^*)_2(\text{OMes})\text{U}(\text{O})]$ (Mes = 2,4,6-trimethylphenyl).²⁵ Although the uranium oxo moiety is well-known for uranyl species, featuring the uranium(VI) trans-dioxo unit $[\text{O}=\text{U}=\text{O}]^{2+}$, the formation of a single terminal oxo unit on monomeric uranium(V) is exceedingly rare, with only the previously cited example crystallographically characterized.

The driving force for the observed multiple bond metathesis leading to the stable terminal oxo species from the metal imido compound is likely the formation and release of the thermodynamically stable isocyanate, R–NCO (Scheme 2). The stability of the resulting terminal oxo species is rather remarkable, as it indicates that this ligand system can support uranium centers with typically very reactive terminal functionalities. In comparison, treating the uranium(III) precursor complex $[(^t\text{BuArO})_3\text{tacn}]\text{U}$ with CO₂ or standard O-atom transfer reagents exclusively leads to formation of dinuclear U(IV/IV) μ -oxo bridged compounds, as a result of the presence of the low valent uranium(III) starting material in solution.⁵ This type

of bimolecular decomposition chemistry is reminiscent of attempts to generate high valent oxo complexes of early first-row transition metals. However, employing a high valent uranium precursor in a metathesis-type reaction eliminates this possibility, preserving the unusual terminal oxo species in complexes of $[(^t\text{RArO})_3\text{tacn}]\text{U}(\text{O})$ for further exploration of electronic structure and oxidation chemistry.

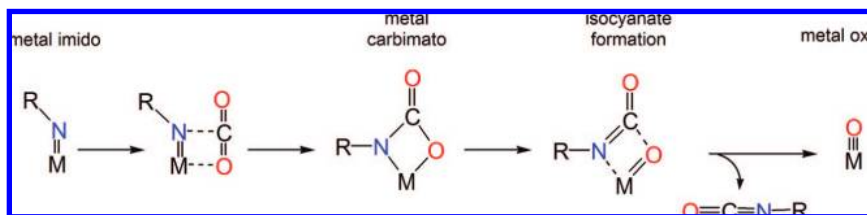
While formation of high valent U=O complexes from carbon dioxide has previously not been reported for uranium complexes, similar chemistry has been observed with transition metals, in particular with the chemically similar titanium ion. Mindiola and co-workers reported the reaction of carbon dioxide with a zwitterionic titanium imido complex, producing the titanium oxo species capped with a borane ligand, namely $[(\text{nacnac})\text{Ti}(\text{OB}(\text{C}_6\text{F}_5)_3)(\text{CH}_3)]$, where (nacnac^-) is $[\text{ArNC}(^t\text{Bu})_2\text{CH}]$; Ar = 2,6-^tPr₂C₆H₃.²⁶ This oxo species is postulated to form via a [2 + 2] cycloaddition pathway, generating a fleeting titanium carbamate species (Scheme 2). Mountford and co-workers were able to isolate and crystallographically characterize intermediate high valent titanium carbamate complexes, produced by addition of carbon dioxide to the titanium imido species, $[(\text{Me}_n\text{taa})\text{Ti}(\text{NR})]$ ($\text{H}_2\text{Me}_n\text{taa}$ = tetra- or octa-methyldibenzotetraaza¹⁴ annulene, $n = 4$ or 8), where R = ^tBu, Ph, Tol or 4-C₆H₄NO₂.²⁷ Transition metal-carbimate compounds formed by the addition of CO₂ to imido species have also been reported for molybdenum,^{28,29} rhenium,³⁰ niobium,³¹ iridium,³² nickel,^{33–35} and tungsten.^{36–39} Catalytic production of carbodiimides from vanadium oxo and imido complexes as well as isocyanates has been achieved and is also indicative of a metathesis pathway via an intermediate vanadium carbamate species.^{40,41}

On the basis of the above-described reports on titanium, a [2 + 2] cycloaddition mechanism is proposed for the formation of the uranium oxo complexes presented here and is further supported by recent work from Boncella. This work describes the addition of isocyanates to uranium(VI) bis(imido) species that results in [2 + 2] cycloaddition to generate different

- (26) Kilgore, U. J.; Basuli, F.; Huffman, J. C.; Mindiola, D. J. *Inorg. Chem.* **2006**, *45*, 487–489.
- (27) Blake, A. J.; McInnes, J. M.; Mountford, P.; Nikonov, G. I.; Swallow, D.; Watkin, D. J. *J. Chem. Soc., Dalton Trans.* **1999**, 379–391.
- (28) Jernakoff, P.; Geoffroy, G. L.; Rheingold, A. L.; Geib, S. J. *J. Chem. Soc., Chem. Commun.* **1987**, 1610–1611.
- (29) Pilato, R. S.; Housmekerides, C. E.; Jernakoff, P.; Rubin, D.; Geoffroy, G. L.; Rheingold, A. L. *Organometallics* **1990**, *9*, 2333.
- (30) Kusthardt, U.; Hermann, W. A.; Ziegler, M. L.; Zahn, T.; Nuber, B. *J. Organomet. Chem.* **1986**, *311*, 163.
- (31) Blacque, O.; Brunner, H.; Kubicki, M. M.; Leblanc, J.-C.; Meier, W.; Moise, C.; Mugnier, Y.; Sadorge, A.; Wachter, J.; Zabel, M. *J. Organomet. Chem.* **2001**, *634*, 47.
- (32) Glueck, D. S.; Wu, J.; Hollander, F. J.; Bergman, R. G. *J. Am. Chem. Soc.* **1991**, *113*, 2041.
- (33) Lemke, F. R.; DeLaet, D. L.; Gao, J.; Kubiak, C. P. *J. Am. Chem. Soc.* **1988**, *110*, 6904–6906.
- (34) DeLaet, D. L.; Fanwick, P. E.; Kubiak, C. P. *J. Chem. Soc., Chem. Commun.* **1987**, 1412.
- (35) DeLaet, D. L.; del Rosario, R.; Fanwick, P. E.; Kubiak, C. P. *J. Am. Chem. Soc.* **1987**, *109*, 754–758.
- (36) Ward, B. D.; Orde, G.; Clot, E.; Cowley, A. R.; Gade, L. H.; Mountford, P. *Organometallics* **2005**, *24*, 2368–2385.
- (37) Darensbourg, D. J.; Frost, B. J.; Larkins, D. L. *Inorg. Chem.* **2001**, *40*, 1993–1999.
- (38) Chisholm, M. H.; Extine, M. W. *J. Am. Chem. Soc.* **1977**, *99*, 782–792.
- (39) Chisholm, M. H.; Extine, M. W. *J. Am. Chem. Soc.* **1977**, *99*, 792–802.
- (40) Birdwhistell, K. R.; Boucher, T.; Ensminger, M.; Harris, S.; Johnson, M.; Toporek, S. *Organometallics* **1993**, *12*, 1023–1025.
- (41) Birdwhistell, K. R.; Lanza, J.; Pasos, J. *J. Organomet. Chem.* **1999**, *584*, 200–205.

(25) Arney, D. S. J.; Burns, C. J. *J. Am. Chem. Soc.* **1993**, *115*, 9840.

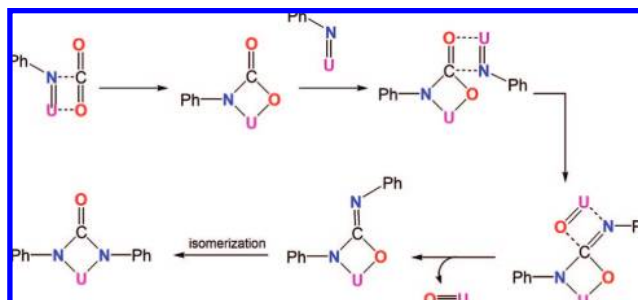
Scheme 2. Mechanistic Possibility for Formation of Metal Carbimato Species via [2 + 2] Cycloaddition



uranium imido species by ligand exchange. In these cases, uranium oxo derivatives were not observed, and the isocyanate is the source for imido fragment exchange.⁴²

In attempts to observe the intermediate uranium(V) carbamate species, the influence of steric pressure on the multiple bond metathesis was tested. Since a decrease in steric bulk was predicted to slow down the loss of isocyanate, a uranium complex with the less bulky, unsubstituted phenyl imido ligand was synthesized. Addition of phenyl azide to the sterically less encumbered uranium(III) complex **1-Bu** yielded the corresponding phenyl imido complex, $[(^t\text{BuArO})_3\text{tacn}]\text{U}(\text{NPh})$ (**3-Bu**) as a brown solid. This complex was fully characterized and showed spectroscopic parameters similar to the mesityl derivative, $[(^t\text{BuArO})_3\text{tacn}]\text{U}(\text{NMes})$ (**2-Bu**) (see Supporting Information, Figures S6 and S7). Addition of carbon dioxide to a brown toluene solution of **3-Bu** immediately produced a dark insoluble solid that was isolated by vacuum filtration. Dissolution of the solid in THF followed by filtration yielded an orange product on the filter assigned as the known oxo complex **4-Bu**. Additionally, black crystals were obtained from the dark THF filtrate and an X-ray diffraction analysis revealed the diphenyl ureate derivative, $[(^t\text{BuArO})_3\text{tacn}]\text{U}(\kappa^2\text{-N,N-(NPh)}_2\text{CO})$ (**5-Bu**) (Figure 3). This complex is eight-coordinate with both urea nitrogen atoms coordinated to the uranium center. The average ligand uranium distances in **5-Bu** are as expected with respective $\text{U}-\text{O}(\text{ArO})_{\text{av}}$ and $\text{U}-\text{N}(\text{tacn})_{\text{av}}$ bond lengths of 2.14 and 2.76 Å. The diphenyl ureate ligand has very similar $\text{U}-\text{N}(\text{ureate})$ distances of 2.329(4) and 2.310(4) Å, slightly longer than expected for $\text{U}-\text{N}$ single bonds (vide supra). In addition, the $\text{C}-\text{O}$ bond distance of 1.225(6) Å is consistent with the formulation as a double bond within the ureate ligand.

Although unexpected, the formation of **5-Bu** indicates that the initial metathesis reaction with carbon dioxide indeed pro-

Scheme 3. Possible Mechanism for Formation of the Diphenyl Ureate Derivative, $[(^t\text{BuArO})_3\text{tacn}]\text{U}(\kappa^2\text{-N,N-(NPh)}_2\text{CO})$ (**5-Bu**)

duces the previously proposed uranium(V) carbamate (Scheme 3). This intermediate carbamate is stable to isocyanate loss but it is still highly reactive and undergoes a second [2 + 2] cycloaddition with another equivalent of uranium(V) phenyl imido species present in solution to form the N,O-diphenyl ureate. Finally, isomerization of this N,O-coordinated species yields the observed N,N-diphenyl ureate derivative **5-Bu** (see Supporting Information for proposed mechanism, Figure S8). Interestingly, both the N,N- and N,O-coordinated diaryl ureate uranium species have been proposed as intermediates in the [2 + 2] cycloaddition of uranium(VI) imido complexes with isocyanates reported by Boncella et al.⁴² Computation using the hybrid DFT level of theory shows that for these uranium(VI) imido compounds, the N,N-bound ureate derivative is lower in energy.⁴² Given that the N,O-ureate derivative is never observed, this energetic difference most likely accounts for the isomerization to the isolated N,N- bound derivative. The formation $[(^t\text{BuArO})_3\text{tacn}]\text{U}(\kappa^2\text{-N,N-(NPh)}_2\text{CO})$ by two consecutive multiple bond metatheses indirectly supports the presence of the proposed uranium(V) carbamate intermediate. However, this species could also have been formed by the reaction of the starting imido complex with PhNCO produced in the reaction.

Synthesis and Characterization of Uranium(IV) Complexes. In an effort to further understand the reactivity of carbon dioxide with $\text{U}-\text{N}$ bonds, the reactivity of the analogous uranium(IV) amide complexes with CO_2 was also investigated. Because of the presence of an additional hydrogen atom on the amide ligand, isocyanate formation and extrusion from these complexes is not possible and may allow retention of the seventh ligand. To preserve the steric integrity of the system, the analogous uranium(IV) mesityl amido species, $[(^R\text{ArO})_3\text{tacn}]\text{U}(\text{NHMe})$ ($\text{R} = ^t\text{Bu}$ (**6-Bu**), Ad (**6-Ad**)), were synthesized by heating 2,4,6-trimethylaniline and the uranium(III) $[(^R\text{ArO})_3\text{tacn}]\text{U}$ compounds to 100 °C (Scheme 4). Amido formation from amines with concurrent loss of 0.5 equiv of dihydrogen is well precedented for low valent uranium⁴³ and other f-block elements.⁴⁴

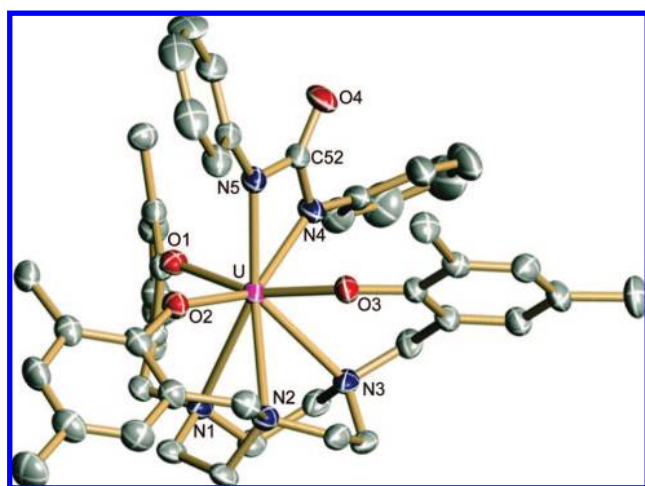


Figure 3. Molecular structure of $[(^t\text{BuArO})_3\text{tacn}]\text{U}(\kappa^2\text{-N,N-(NPh)}_2\text{CO})$ (**5-Bu**) in crystals of **5-Bu** · 3*n*-C₅H₁₂ shown with 50% probability ellipsoids. Hydrogen atoms, solvent molecules, and *tert*-butyl substituents are omitted for clarity.

(42) Spencer, L. P.; Yang, P.; Scott, B. L.; Batista, E. R.; Boncella, J. M. *J. Am. Chem. Soc.* **2008**, *130*, 2930–2931.

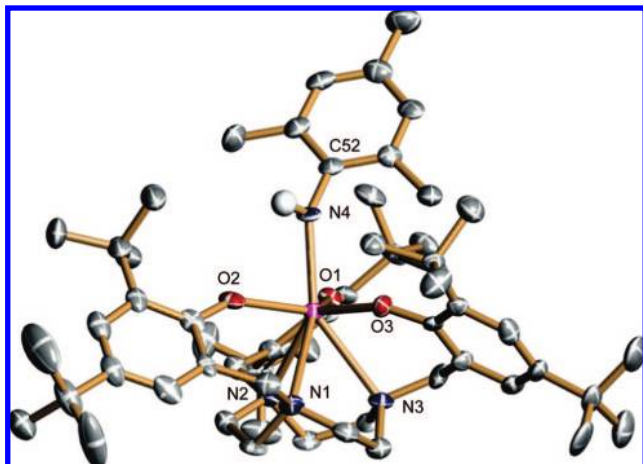


Figure 4. Molecular structure of $[(^t\text{BuArO})_3\text{tacn})\text{U}(\text{NHMe})]$ (**6-Bu**) in crystals of **6-Bu**·Et₂O shown with 50% probability ellipsoids. Selected hydrogen atoms and solvent molecules are omitted for clarity.

Single crystals of $[(^R\text{ArO})_3\text{tacn})\text{U}(\text{NHMe})]$ suitable for X-ray diffraction analysis were grown by cooling a concentrated pentane solution of **6-Bu** to -35°C . Analysis revealed a seven coordinate uranium(IV) amido species with its signature core complex $[(^R\text{ArO})_3\text{tacn})\text{U}]$ and the axially bound MesNH amido group (Figure 4). The U–N(amido) bond length of 2.305(6) Å is as expected, and significantly longer than that of the corresponding U–N(imido) distance in the previously discussed uranium(V) imido complex **2-Bu** ($d(\text{U}–\text{N}(\text{imido})) = 2.047(8)$ Å), supporting the assignment of **6-Bu** as a distinct U(IV) amide compound. The observed U–N(amido) distance in **6-Bu** is long compared to those reported for other uranium amide derivatives, such as $[(\eta^5\text{-C}_5\text{Me}_5)_2\text{U}(\text{Cl})(\text{NH}(p\text{-C}_6\text{H}_5\text{C}_1))]^{45}$ and $[(\eta^5\text{-C}_5\text{Me}_5)_2\text{U}(\text{NH}(2,6\text{-Me}_2\text{C}_6\text{H}_3))]^{46}$ which have similar amide ligands with respective U–N bond distances of 2.237(3) Å and 2.267(6) Å. The U–N–C angle is $142.1(5)^\circ$, as is expected for an sp^2 -hybridized amide nitrogen. The respective U–O(ArO)_{av} and U–N(tacn)_{av} distances are 2.19 and 2.68 Å, and the displacement of the uranium below the plane of the three aryloxy oxygen atoms in **6-Bu** is 0.234(3) Å, as is expected for uranium(IV) ions stabilized by this ligand set.¹⁶

Exposure of a toluene solution of orange **6-Bu** to an atmosphere of carbon dioxide produced an immediate color change to light green (Scheme 4). After removal of the solvent *in vacuo*, the residue was triturated with pentane and a light pink precipitate (**7-Bu**) was isolated by vacuum filtration. Analysis by IR spectroscopy showed an $\nu(\text{N}–\text{H})$ absorption centered at 3438 cm^{-1} and an additional strong band at 1651 cm^{-1} , assigned as the C=O stretch of an $\eta^1\text{-O}$ bound, monodentate carbamate ligand, $\eta^1\text{-OC(O)N(H)Mes}$.⁴⁷

Pink block-shaped crystals suitable for X-ray crystallography were grown from diffusion of pentane into a saturated solution of **7-Bu** in diethyl ether. Analysis confirmed the insertion of carbon dioxide into the U–N(amide) bond to form the ura-

nium(IV) carbamate species, $[(^t\text{BuArO})_3\text{tacn})\text{U}(\eta^1\text{-OC(O)N}(\text{H)Mes})]$ (**7-Bu**) (Figure 5, metrical parameters in Table 2). The uranium is seven-coordinate, and only one of the C–O groups of the carbamate ligand is coordinated to the uranium center. The uranium ligand distances are in the expected range for this ligand set, with average U–O(Ar)_{av} and U–N(tacn)_{av} distances of 2.18 and 2.66 Å, respectively. The U–O distance for the coordinated carbamate ligand is 2.227(3) Å, indicating a single bond. The C–O bond length for the uranium-coordinated oxygen is 1.287(5) Å, while the C–O distance in the uncoordinated ketyl group is shorter at 1.196(5) Å, as expected for a C=O double bond. In addition, the C(carbamate)–N bond distance is 1.422(5) Å, which would be predicted for a C–N single bond. The uranium is located below the trigonal plane of the three aryloxy oxygen atoms by 0.259(2) Å, similar to the displacement found in the uranium(IV) starting material (**6-Bu**).

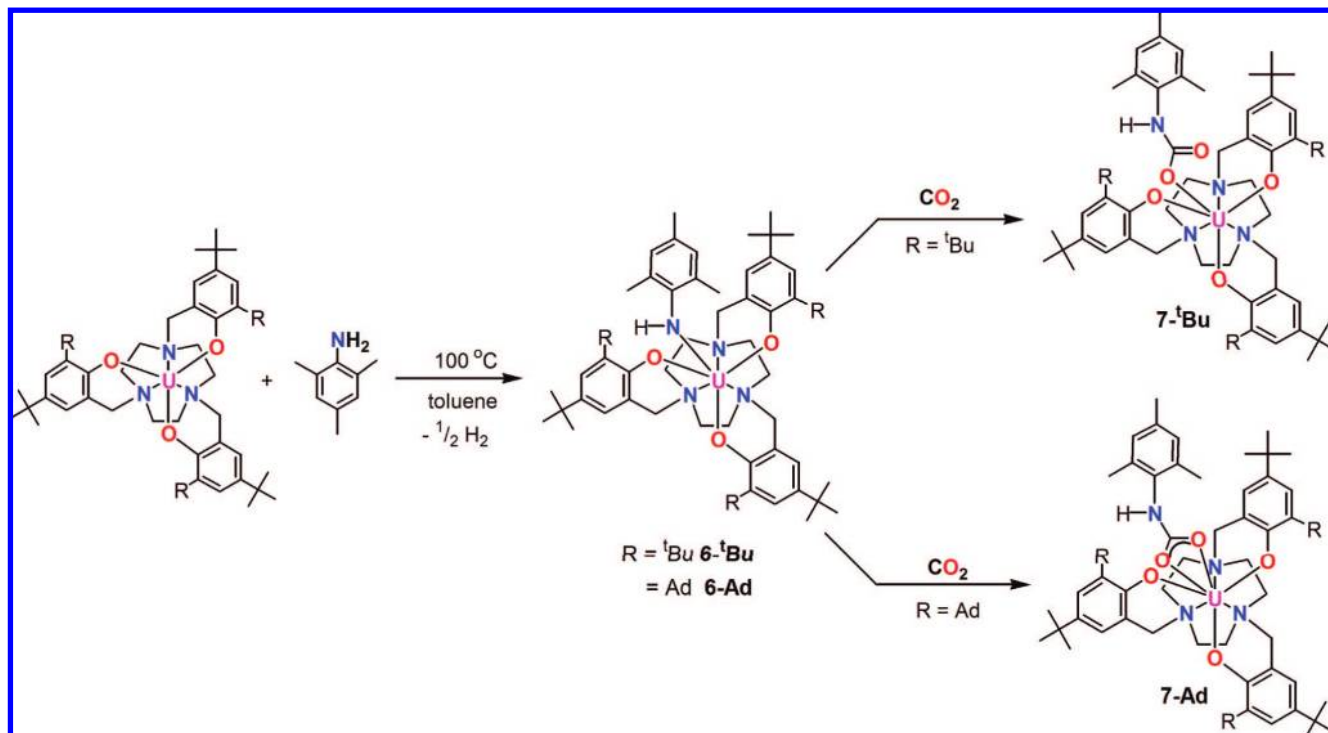
Because of the high solubility of the uranium amido complex (**6-Ad**), purification for full spectroscopic characterization was not accomplished. Nevertheless, reactivity studies of this complex were pursued. Accordingly, exposure of an orange solution of **6-Ad** to CO₂ produced a color change to light green (Scheme 4). Removal of the solvent *in vacuo* left a green residue, assigned as the carbamate complex $[(^{\text{Ad}}\text{ArO})_3\text{tacn})\text{U}(\text{OC(O)N}(\text{H)Mes})]$ (**7-Ad**). In contrast to **7-Bu**, no features were observed in the infrared spectrum in the region expected for carbonyl vibrational stretches. X-ray diffraction of green crystals, grown from a benzene/acetonitrile solution, confirmed the insertion of carbon dioxide into the U–N bond, but with a different coordination mode than **7-Bu** (Figure 6, metrical parameters in Table 2). In this case, both oxygen atoms of the carbamate ligand are coordinated to the uranium center in a bidentate $\kappa^2\text{-O}_2\text{CN}(\text{H)Mes}$ fashion, resulting in the eight-coordinate uranium carbamate species, $[(^{\text{Ad}}\text{ArO})_3\text{tacn})\text{U}(\kappa^2\text{-O}_2\text{CN}(\text{H)Mes})]$ (**7-Ad**). The carbamate ligand has U–O bond distances of 2.434(4) Å and 2.527(4) Å, O–C distances of 1.259(7) and 1.278(7) Å, and an N–C distance of 1.383(7) Å. The displacement of the uranium center from the trigonal aryloxy plane, $d(\text{U}–\text{O}_{\text{opp}})$, is 0.187(2) Å, which is significantly smaller than that found for the uranium(IV) precursor **6-Bu** ($d(\text{U}–\text{O}_{\text{opp}}) = 0.234(3)$ Å) and the carbamate complex **7-Bu** of the related *tert*-butyl system ($d(\text{U}–\text{O}_{\text{opp}}) = 0.259(2)$ Å).

The different coordination modes observed for the two carbamate ligands in **7-Bu** and **7-Ad** are most likely due to the steric differences of the macrocyclic ligand framework. In the case of **7-Bu**, the monodentate carbamate ligand features a short uranium oxygen distance of 2.227(3) Å. This is possible because of the relatively open cavity of this molecule, which allows close approach of the carbamate ligand to the uranium center for stronger coordination. However, in the case of **7-Ad**, the carbamate ligand is unable to approach the uranium center closely enough to form a strong bond due to the bulky adamantyl substituents protecting the uranium ion. As a result, two weaker bonds with distances of 2.434(4) Å and 2.527(4) Å are formed to compensate for this inability to form a single strong bond to the electropositive uranium ion.

In addition to complexes **7-Bu** and **7-Ad**, few other examples of uranium(IV) carbamate complexes are reported in the literature. Calderazzo reports IR spectroscopic evidence for the formation of the tetracarbamate compound $[\text{U}(\text{O}_2\text{CNEt}_2)_4]$, generated by addition of diethylamine and carbon dioxide to a toluene solution of UCl₄.⁴⁸ Mechanistic studies support that formation of this complex occurs via initial generation of the

- (43) Lam, O. P.; Feng, P. L.; Heinemann, F. W.; O'Connor, J. M.; Meyer, K. *J. Am. Chem. Soc.* **2008**, *130*.
 (44) Evans, W. J.; Kociok-Koehn, G.; Leong, V. S.; Ziller, J. W. *Inorg. Chem.* **1992**, *31*, 3592.
 (45) Peters, R. G.; Scott, B. L.; Burns, C. J. *Acta Crystallogr., Sect. C* **1999**, *C55*, 1482–1483.
 (46) Straub, T.; Frank, W.; Reiss, G. J.; Eisen, M. S. *J. Chem. Soc., Dalton Trans.* **1996**, 2541.
 (47) Arduini, A. L.; Jamerson, J. D.; Takats, J. *Inorg. Chem.* **1981**, *20*, 2474.

Scheme 4. Synthesis of Uranium(IV) Amido Complexes, $[(^R\text{ArO})_3\text{tacn}]\text{U}(\text{NHMe})$ ($\text{R} = \text{}^t\text{Bu}$ (**6- ^tBu**); Ad (**6-Ad**)) and Uranium(IV) Carbamate Species, $[(^R\text{ArO})_3\text{tacn}]\text{U}(\text{O}_2\text{CNHMe})$ ($\text{R} = \text{}^t\text{Bu}$ (**7- ^tBu**); Ad (**7-Ad**))



dialkylammonium carbamate *in situ*, followed by salt metathesis with uranium(IV) chloride generating the observed product and ruling out insertion of carbon dioxide into the U–N bond as observed for **7- ^tBu** and **7-Ad**. A vibrational band at 1510 cm^{-1} was assigned to the C–N stretch in the IR spectrum for $[\text{U}(\text{O}_2\text{CNET}_2)_4]$ in noncoordinating solvents, consistent with formation of a bidentate carbamate species. When donor solvents are used, an additional peak at 1700 cm^{-1} appears due to the C=O stretch of a monodentate carbamate ligand, which forms in the presence of these solvents. Regardless, no crystallographic evidence was provided to confirm these coordination modes. Insertion of carbon dioxide does occur, however, in the case of $[(\eta^5\text{-C}_5\text{H}_5)_2\text{U}(\text{NET}_2)_2]$ to form the corresponding car-

Table 2. Selected Distances (Å) for Uranium(IV) Complexes

structural parameters	6-^tBu	7-^tBu	7-Ad
U–N _{1,tacn}	2.646(5)	2.666(3)	2.729(4)
U–N _{2,tacn}	2.730(6)	2.715(3)	2.751(4)
U–N _{3,tacn}	2.686(6)	2.616(3)	2.565(4)
U–N _{av}	2.69	2.66	2.68
U–O _{1,ArO}	2.214(5)	2.190(3)	2.197(4)
U–O _{2,ArO}	2.214(5)	2.160(3)	2.149(4)
U–O _{3,ArO}	2.151(5)	2.179(3)	2.214(4)
U–O _{av}	2.19	2.18	2.19
U–N _{amide}	2.305(6)		
U–O _{carbamate}		2.227(3)	2.434(4)
			2.527(4)
O–C _{carbamate}		1.287(5)	1.259(7)
		1.196(5) (free)	1.278(7)
C–N _{carbamate}		1.375(5)	1.383(7)
N–C _{mesityl}		1.422(5)	1.421(8)
U _{out-of-plane shift}	0.234(3)	0.259(2)	0.187(2)

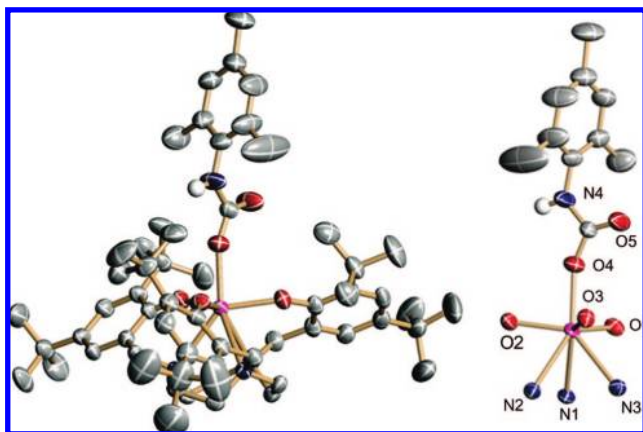


Figure 5. Molecular structure of $[(^t\text{BuArO})_3\text{tacn}]\text{U}(\text{CO}_2\text{NHMe})$ (**7- ^tBu**) in crystals of **7- ^tBu** · $2\text{Et}_2\text{O}$ (left), with core structure of **7** (right) shown with 50% probability ellipsoids. Selected hydrogen atoms and solvent molecules are omitted for clarity.

bamate species, $[(\eta^5\text{-C}_5\text{H}_5)_2\text{U}(\text{O}_2\text{CNET}_2)_2]$ as demonstrated by Takats.⁴⁷ On the NMR time scale, the coordinated carbamate is dynamic in solution. Although spectroscopic characterization confirmed the bidentate coordination mode of the carbamate ligand, X-ray diffraction data of this compound also was not reported. Crystallographic evidence for similar insertion chemistry was observed for tetrakis(dialkylamido) uranium(IV) derivatives to produce uranium carbamate clusters,⁴⁹ but the molecular structures presented for compounds **7- ^tBu** and **7-Ad** represent, to the best of our knowledge, the first examples of crystallographically characterized monomeric uranium carbamate species. These uranium(IV) carbamate species demonstrate the ability of carbon dioxide to insert into the U–N amide bond

(48) Calderazzo, F.; Dell'Amico, G.; Netti, R.; Pasquali, M. *Inorg. Chem.* **1978**, *17*, 471–473.

(49) Calderazzo, F.; Dell'Amico, G.; Pasquali, M.; Perego, G. *Inorg. Chem.* **1978**, *17*, 474.

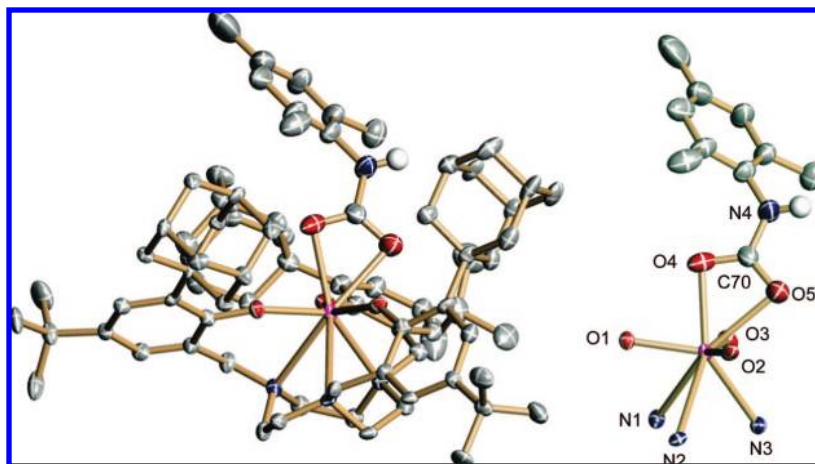


Figure 6. Molecular structure of $[(^{\text{Ad}}\text{ArO})_3\text{tacn})\text{U}(\text{CO}_2\text{NHMe})]$ (**7-Ad**) in crystals of **7-Ad**·0.625Et₂O·1.375 MeCN (left) and core structure of **7-Ad** (right) shown with 50% probability ellipsoids. Selected hydrogen atoms and solvent molecules are omitted for clarity.

of $[(^{\text{R}}\text{ArO})_3\text{tacn})\text{U}(\text{NHMe})]$ ($\text{R} = \text{tBu, Ad}$). Loss of isocyanate drives the uranium(V) reaction to proceed, precluding the isolation of the carbamate species formed from carbon dioxide insertion into the uranium nitrogen imido bond. However, with an additional hydrogen present in complexes **6-tBu** and **6-Ad**, isocyanate formation is not possible and the carbon dioxide insertion products **7-tBu** and **7-Ad** are observable.

Electronic Structure of Uranium(V) Complexes. To more fully understand the uranium(V) complexes, their electronic structures were studied using a number of techniques, including electronic absorption and EPR spectroscopies, as well as magnetization studies and DFT calculations, and these results compared to previously synthesized complexes.

The electronic absorption spectra of the dark brown imido complexes, **2-tBu** and **2-Ad** (in toluene), and the bright orange oxo complexes, **4-tBu** and **4-Ad** (in acetonitrile), were acquired from 300 to 2100 nm. An overlay comparing the spectra of **2-tBu** and **4-tBu** is presented in Figure 7. The corresponding spectra of the similar adamantane derivatized complexes **2-Ad** and **4-Ad** are provided in the Supporting Information (Figure S2). The spectra of the imido complexes **2-tBu** and **2-Ad** both show intense ligand-to-metal charge-transfer bands (LMCT). One of these bands appears in the near UV region with a shoulder at approximately 370 nm ($\epsilon \approx 6700 \text{ cm}^{-1} \text{ M}^{-1}$) and a very broad feature in the NIR range of the spectrum is centered at $\lambda_{\text{max}} \approx 980 \text{ nm}$ ($\epsilon \approx 600 \text{ cm}^{-1} \text{ M}^{-1}$). Except for some weak unresolved fine structure, most likely stemming from underlying f–f transitions, the latter broad band is mostly featureless. This broadband is unique as it cannot be observed in other uranium(V) imido complexes of the $(^{\text{R}}\text{ArO})_3\text{tacn}^{3-}$ ligand system synthesized to date, including $[(^{\text{R}}\text{ArO})_3\text{tacn})\text{U}(\text{NR}^{\prime})]$ complexes with $\text{R}^{\prime} = \text{SiMe}_3$, Ad, or CPh_3 .¹⁶ These previously reported uranium(V) imido complexes range in color from dark green to green-brown.^{16,24} They exhibit characteristic electronic absorption spectra with relatively intense and broad charge transfer bands between 300 and 600 nm and less intense relatively sharp bands ($\epsilon \leq 200 \text{ M}^{-1} \text{ cm}^{-1}$) arising from metal-centered f–f transition at higher wavelengths up to 2100 nm.

The uranium(V) oxo complexes **4-tBu** and **4-Ad** also do not possess this intense LMCT band but exhibit a different, very unique set of absorption bands. Instead of broad and intense LMCT bands in the visible and NIR, four sharp, low-intensity bands at $\lambda_{\text{max}} = 1770 \text{ nm}$ ($\nu = 5650 \text{ cm}^{-1}$, $\epsilon = 70 \text{ cm}^{-1} \text{ M}^{-1}$), 1480 nm ($\nu = 6769 \text{ cm}^{-1}$, $\epsilon = 90 \text{ cm}^{-1} \text{ M}^{-1}$), 1205 nm ($\nu =$

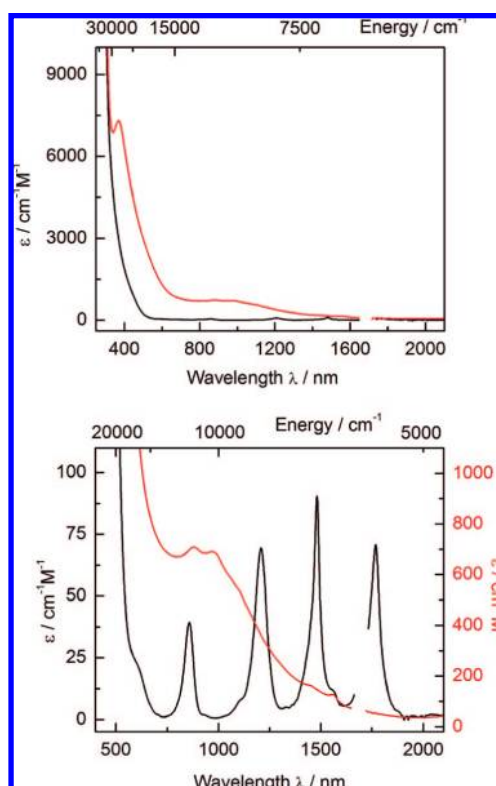


Figure 7. Electronic absorption spectra of **2-tBu** (red trace) and **4-tBu** (black trace) recorded in toluene and acetonitrile from 300 to 2100 nm (top, low concentration) and 450 to 2100 nm (bottom, high concentration).

8300 cm^{-1} , $\epsilon = 75 \text{ cm}^{-1} \text{ M}^{-1}$), and 850 nm ($\nu = 11765 \text{ cm}^{-1}$, $\epsilon = 50 \text{ cm}^{-1} \text{ M}^{-1}$) are observed as well as a shoulder at 585 nm ($\nu = 17100 \text{ cm}^{-1}$, $\epsilon \approx 23 \text{ cm}^{-1} \text{ M}^{-1}$) located near the onset of the charge transfer band in the near UV region of the spectrum. These distinct absorption bands appear to arise from f–f transitions and have not been observed in any other uranium(V) complex of the $[(^{\text{R}}\text{ArO})_3\text{tacn})\text{U}]$ type, and hence, appear to be characteristic for the here presented uranium(V) oxo complexes. However, the maximum number of electronic transitions that should be observed in this region is four (see below), so further low temperature optical investigations (including temperature- and field-dependent MCD) are planned and will be reported separately in due time. It is plausible that

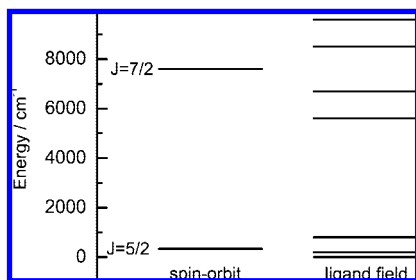


Figure 8. Schematic energy levels for a $5f^1$ system assuming the spin-orbit interaction is much greater than the ligand field interaction.

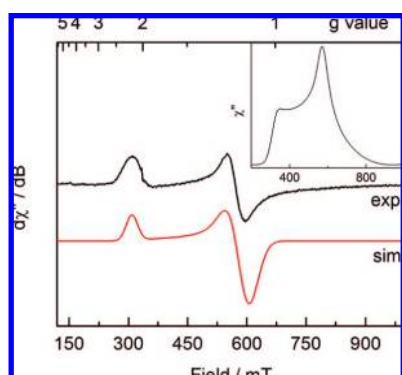


Figure 9. X-Band EPR spectrum of **4-Ad**, recorded in a toluene/acetonitrile glass at 5 K ($\nu = 9.40187$ GHz, $P = 0.10$ mW, modulation = 3.0 mT at 100 kHz). The spectrum was simulated with $g_{\perp} = 1.14$ and $g_{\parallel} = 2.15$ and Gaussian lines with $W_{\perp(\text{fwhm})} = 32.0$ and $W_{\parallel(\text{fwhm})} = 17.0$ mT. The inset shows a numerical integration of the experimental derivative spectrum obtained with a minor linear correction of the baseline.

the more ionic $\text{U}=\text{O}$ metal–ligand interaction in **4-Bu** and **4-Ad** results in a blue-shift of the ligand-to-metal charge-transfer bands observed at lower energy for the isoelectronic uranium(V) imido complexes. The absorption spectra of the uranium(V) imido and oxo complexes reported here are notably different and have significantly different electronic structures and reactivity compared to the previously known U(V) complexes of this ligand system.

From the ligand field theory for U(V) compounds, the 2F manifold of a $5f$ electron will be split by the $5f$ spin-orbit interaction into two J multiplets, $J = ^5/2, ^7/2$ (Figure 8). From the free ion data for the U^{5+} ion, the spin-orbit coupling constant is $\zeta = 2173.9 \text{ cm}^{-1}$.⁵⁰ Each of these J levels will be split further by the ligand (or crystal field) into $(2J + 1)/2$ doubly degenerate levels. Assuming the U^{5+} ion is at a site of approximately C_{3v} symmetry (as found exactly for **4-Bu** and approximately for **4-Ad**) the $J = ^5/2$ multiplet will split into two $\mu = ^1/2$ (Γ_4 symmetry) doublets and one $\mu = ^3/2$ (Γ_5, Γ_6 symmetry) doublet. The $J = ^7/2$ multiplet will split into two $\mu = ^1/2$ doublets and two $\mu = ^3/2$ doublets.⁵¹ Assuming the spin-orbit interaction is much greater than the ligand field interaction and of the magnitude found for the free ion, we would expect the energy level diagram presented in Figure 9 for these systems. With this picture we would expect to observe optical transitions in the $5500\text{--}10000 \text{ cm}^{-1}$ range, as found for **4-Ad** and **4-Bu** (Figure 7).

To obtain a more comprehensive picture of the unique electronic structure, the newly synthesized uranium(V) imido

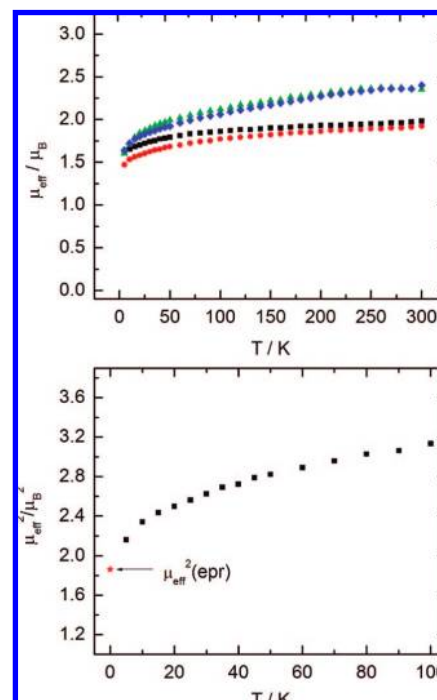


Figure 10. Temperature-dependent SQUID magnetization data (at 1 T) for samples of $[\text{U}(\text{ArO})_3\text{tacn}]\text{U}(\text{NMes})$ (**2-Bu**) (green circles), $[\text{U}(\text{ArO})_3\text{tacn}]\text{U}(\text{NMes})$ (**2-Ad**) (blue squares), $[\text{U}(\text{ArO})_3\text{tacn}]\text{U}(\text{O})$ (**4-Bu**) (black diamonds), and $[\text{U}(\text{ArO})_3\text{tacn}]\text{U}(\text{O})$ (**4-Ad**) (red triangles) plotted as a function of magnetic moment (μ_{eff}) vs temperature (T). Data were corrected for underlying diamagnetism (top). Plot of μ_{eff}^2 vs temperature for **4-Ad** showing the calculated value at 0 K as determined from EPR spectroscopy (bottom).

and oxo complexes were also studied by low-temperature X and S-band EPR spectroscopy and variable temperature SQUID magnetization. Analysis of toluene/acetonitrile glasses of **4-Bu** and **4-Ad** at 5 K produced X-band EPR signals, which decayed in intensity as the temperature was increased and disappeared completely at temperatures above 80 K owing to excessive line broadening. The EPR spectra of **4-Ad** and **4-Bu** at low temperatures (8 K) are shown in Figure 9 and Figure S5. For approximate C_{3v} symmetry, axial spectra are expected and the observed spectra have been assigned. Despite line distortions, possibly due to fast spin-spin relaxation and g -strain, the derivative signal was best fitted as an axial set of g -values with derivative lines centered at $g_{\parallel} = 2.15$ and $g_{\perp} = 1.14$ (Figure 9); no other features were observed at magnetic fields as high as $B_0 \approx 1250$ mT ($g \approx 0.45$). Although this fit does not simulate the experimental derivative spectrum perfectly, the appearance of the absorption spectrum obtained by numerical integration, however, clearly is of axial symmetry (see inset). In C_{3v} symmetry, the $J = ^5/2$ state splits into three magnetic doublets, two EPR active $\mu = \pm^1/2$ and one EPR inactive $\mu = \pm^3/2$ state, where μ is the crystal ground-state number.⁵² Given that the $\mu = ^3/2$ state is EPR silent, the ground-state crystal field of the EPR active compounds examined here must be $\mu = ^1/2$.⁵³ Accordingly, it was suggested that the equally C_{3v} symmetrical but EPR silent uranium(V) imido complexes $[(\eta^5\text{-MeC}_5\text{H}_4)_3\text{U}(\text{NR})]$ and $[(\eta^5\text{-MeC}_5\text{H}_4)_3\text{U}]_2(\mu\text{-N}_2\text{C}_6\text{H}_4)$ studied by Rosen, Andersen, and Edelstein have a $\mu = \pm^3/2$ crystal field ground

(50) Kaufman, V.; Radziemski, L. J. *J. Opt. Soc. Am.* **1976**, *66*, 599.

(51) Koster, G. F.; Dimmock, J. O.; Wheeler, R. G.; Statz, H. *Properties of the Thirty-Two Point Groups*; MIT Press: Cambridge, MA, 1963.

(52) Wybourne, B. G. *Spectroscopic Properties of Rare Earths*; Wiley Interscience: New York, 1963; p 167.

(53) Rosen, R. K.; Andersen, R. A.; Edelstein, N. M. *J. Am. Chem. Soc.* **1990**, *112*, 4588–4590.

state.^{53,54} Similarly, all uranium(V) imido complexes of the $[(\text{ArO})_3\text{tacn}]\text{U}(\text{NR})$ type were found to be EPR-inactive, and so are the uranium(V) imido complexes **2-Bu** and **2-Ad** reported herein. It was therefore rather unexpected to find the structurally and electronically related uranium(V) oxo complexes **4-Bu** and **4-Ad** to be EPR active under the same conditions. A frozen solution of complex **4-Bu** also was studied in the S-band ($\nu = 3.5$ GHz) EPR frequency; however, probably due to the very large line widths, no spectrum was observed.

Reproducible SQUID data were collected for several independently synthesized samples (see Supporting Information, Figures S3 and S4) of U(V) imido complexes **2-Bu** and **2-Ad** as well as oxo complexes **4-Bu** and **4-Ad** over a temperature range of 5–300 K. The effective magnetic moment, μ_{eff} , of **2-Bu** and **2-Ad** exhibits a steady decline as the temperature is lowered, decreasing from the respective values of 2.35 and 2.40 μ_{B} at 300 K to 1.67 and 1.64 μ_{B} at 5 K. This behavior is typical for uranium(V) f^1 complexes. The previously reported trimethylsilyl imido complexes $[(\text{t}^{\text{Bu}}\text{ArO})_3\text{tacn}]\text{U}(\text{NSiMe}_3)$ ¹⁶ and $[(\text{Ad}^{\text{ArO}})_3\text{tacn}]\text{U}(\text{NSiMe}_3)$,²⁴ studied in the same temperature range, have respective values of 1.46–2.34 μ_{B} and 1.42–2.28 μ_{B} . Comparing the U(V) imido complexes **2-Bu** and **2-Ad** to the oxo complexes shows significantly lower effective magnetic moments for **4-Bu** and **4-Ad** and display noticeably less temperature dependency of μ_{eff} in the same temperature range. The *tert*-butyl derivative $[(\text{t}^{\text{Bu}}\text{ArO})_3\text{tacn}]\text{U}(\text{O})$ (**4-Bu**) has values ranging from 1.61 to 1.98 μ_{B} (5 to 300 K), while those of $[(\text{Ad}^{\text{ArO}})_3\text{tacn}]\text{U}(\text{O})$ (**4-Ad**) are ranging from 1.49 to 1.92 μ_{B} (Figure 10). The effective magnetic moments reported for uranium(V) complexes are generally smaller than the theoretical value of 2.54 μ_{B} predicted for the free ion from the $L-S$ coupling scheme. For high valent uranium complexes, which are often stabilized by strongly π -donating ligands, such as terminal oxo or imido ligands, Boudreaux and Mulay have attributed this observation to covalency effects originating from strong metal-to-ligand bonding.⁵⁵ The effective magnetic moments at 0 K can be calculated from the measured EPR g -values. For **4-Bu** and **4-Ad** values of $\mu_{\text{eff}} = 1.19 \mu_{\text{B}}$ and $\mu_{\text{eff}} = 1.36 \mu_{\text{B}}$ were obtained. These values are in fair agreement with the extrapolated values obtained from the experimental susceptibility data. This can be further illustrated by plotting the data as a function of μ_{eff}^2 vs temperature as presented in Figure 10 (bottom). Here, the last point with a value of 1.862 μ_{B}^2 at 0 K is in good agreement with the extrapolated experimental data. The magnetic susceptibility data clearly show that one or more of the higher lying crystal field states of the $J = 5/2$ multiplet contribute to the magnetism in the experimental temperature range 2–300 K.

The electronic structure of the uranium(V) oxo complex, **4-Bu** was also investigated by Kohn–Sham DFT using the ADF package (version 2007.01).^{56–58} Analyses and geometry optimizations were performed employing the BP86 gradient cor-

Table 3. Optimized Selected Distances (Å) and Angles (deg) for Uranium(V) Complexes

structural parameters	4-Bu	
	theory	experiment
U–N _{av}	2.776	2.676(6)
U–O _{av}	2.208	2.203(5)
U–N _{imido}	1.993	2.047(8)
U–N–C _{imido}	160.4	154.7(8)
U–O _{oxo}	1.854	1.848(7)

rected functional^{59,60} in the scalar zeroth-order regular approximation^{61–63} (ZORA). The basis set applied is of TZP quality with frozen cores for the second row elements (1s) as well as for uranium (including 5d). Selected calculated and experimental geometrical parameters are summarized in Table 3.

A geometry optimization was performed on $[(\text{t}^{\text{Bu}}\text{ArO})_3\text{tacn}]\text{U}(\text{O})$ (**4-Bu**) resulting in close to perfect C_3 symmetry for the molecule. As presented in Table 3, the distances calculated from the optimized structures agree very well with those distances obtained from the crystal structure of **4-Bu**. The scalar ZORA computation reveals that the unpaired electron is in a “ $5f_{x(x^2-3y^2)}$ -like” SOMO, which has 3-fold (φ) symmetry with respect to the uranium oxo axis (Figure 11).^{64,65} Three of the six lobes of this orbital are pointing directly toward the aryloxo oxygen ligands in the plane resulting in a highly antibonding situation. However, this antibonding character of the orbitals is reduced by mixing with 9.7% $5f_z^2$, 7.6% $6d_z^2$ and 4.4% $7s$ of the uranium orbitals along the U–O(ArO) axis resulting in increased electron density pointing down between the tacn nitrogen atoms. This stabilizes the degenerate pair of LUMOs namely $5f_{yz}$ and $5f_{z(x^2-y^2)}$ that are purely uranium f orbital in character. The LUMOs are of δ symmetry with respect to the uranium–oxygen axis, and thus, are essentially nonbonding with regard to the axial oxygen. However, they are slightly π antibonding with respect to the three oxygen atoms in the plane. The four orbitals describing the U=O triple bond are also depicted in Figure 11 (bottom). As expected for uranium(V), these bonds are very polarized toward the oxygen with only minor components of $5f$ and $6d$ uranium orbitals. These polarized bonds are very strong and are found 4–5 eV below the SOMO.

Conclusions

The uranium complexes presented herein represent unique molecules resulting from activation of carbon dioxide with high-valent uranium(V) imido and midvalent uranium(IV) amido species via multiple bond metathesis and CO_2 insertion. The uranium(V) imido complexes have relatively long U–N(imido) bond lengths, making them highly reactive with carbon dioxide. Employing the mesityl imido derivative results in terminal oxo species through facile loss of isocyanate from a uranium(V) carbamate intermediate via multiple bond metathesis. Investigations into the role of size and substitution pattern of the imido

- (54) Brennan, J. G.; Andersen, R. A. *J. Am. Chem. Soc.* **1985**, *107*, 514–516.
 (55) Boudreaux, E. A.; Mulay, L. N. *Theory and Applications of Molecular Paramagnetism*; John Wiley & Sons: New York, 1976; Vol. 510.
 (56) te Velde, G.; Bickelhaupt, F. M.; van Gisbergen, S. J. A.; Fonseca Guerra, C.; Baerends, E. J.; Snijders, J. G.; Ziegler, T. *J. Comput. Chem.* **2001**, *22*, 931.
 (57) Fonseca Guerra, C.; Snijders, J. G.; te Velde, G.; Baerends, E. J. *Theor. Chem. Acc.* **1998**, *99*, 391.
 (58) ADF2007.01, SCM, Theoretical Chemistry, Vrije Universiteit, Amsterdam, The Netherlands, <http://www.scm.com>.

- (59) Becke, A. D. *Phys. Rev. A* **1988**, *38*, 3098.
 (60) Perdew, J. P. *Phys. Rev. B* **1986**, *33*, 8822.
 (61) Van Lenthe, E.; Baerends, E. J.; Snijders, J. G. *J. Chem. Phys.* **1993**, *99*, 4597.
 (62) Van Lenthe, E.; Baerends, E. J.; Snijders, J. G. *J. Chem. Phys.* **1994**, *101*, 9783.
 (63) Van Lenthe, E.; Ehlers, A. E.; Baerends, E. J. *J. Chem. Phys.* **1999**, *110*, 8943.
 (64) Bergman, D. L.; Laaksonen, L.; Laaksonen, A. *J. Mol. Graph. Model.* **1997**, *15*, 301.
 (65) Laaksonen, L. *J. Mol. Graph.* **1992**, *10*, 33.

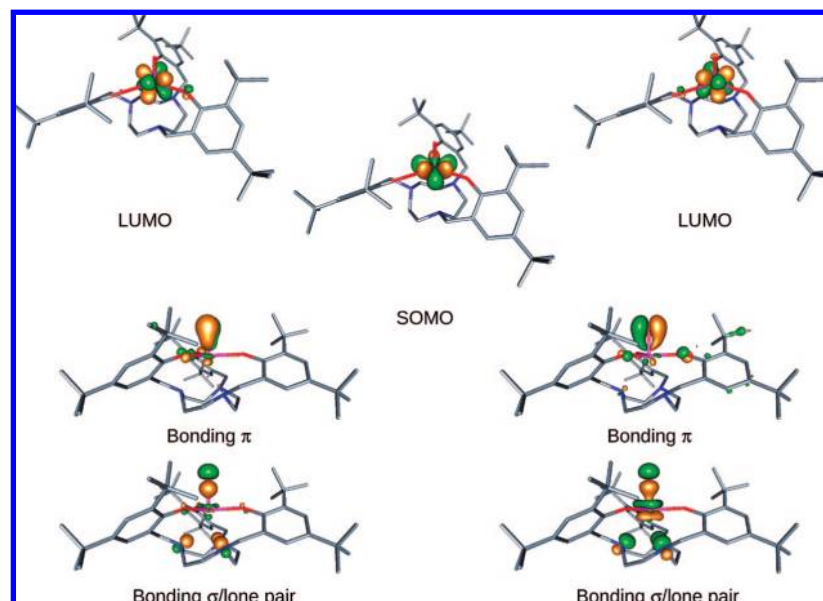


Figure 11. Isosurface plots of the orbitals of 4'-Bu. The degenerate pure uranium f LUMOs (top), followed by the uranium based SOMO (−2.97 eV) and the four bonding uranium oxygen orbitals (bottom).

ligand in the formation of these rare oxo species prompted the use of the sterically less-hindered phenyl imido in an attempt to slow down the rate of isocyanate loss. This variation of starting material has remarkable effects and leads to a rather surprising uranium(V) diaryl ureate generated from two consecutive multiple-bond metathesis reactions. Like the uranium(V) imido complexes, the uranium(IV) amide complexes discussed here also readily react with carbon dioxide but instead yield monomeric uranium(IV) carbamate species formed from insertion into the U–N bond. The crystallographic characterization of both uranium carbamate complexes confirms the CO₂ insertion into the U–N bonds and highlights the differences in coordination mode affected by the steric pressure of the *tert*-butyl and adamantyl groups of the stabilizing tacn chelator.

The new uranium(V) terminal oxo species have distinctive electronic structures not previously observed for uranium(V) complexes. Unlike previously synthesized EPR inactive uranium(V) imido species, these uranium(V) oxo complexes are EPR active, consistent with a $\mu = \pm 1/2$ ground state. As expected from the ligand field splitting diagram provided, their electronic absorption spectra show sharp transition bands throughout the near-infrared region. The data obtained from the EPR spectrum has allowed calculation of the effective magnetic moments at low temperature. Results from DFT calculations show that the unpaired electron is in a “5f_{x²−3y²−like” SOMO, and thus, the unpaired electron is localized in the plane of the aryloxide}

groups of the chelating ligand, and nonbonding with respect to the U≡O moiety.

In summary, the studies presented herein demonstrate that mid- and high-valent uranium centers are highly capable of activating an inert molecule such as carbon dioxide. The oxidation state of the uranium center and the molecular architecture provided by the surrounding ligands have strong influences on the mechanism of activation as well as the final products. Tuning the sterics and electronics of this system allowed the exploration of rare uranium(V) oxo species with an unusual and distinct electronic structure. In depth studies on the electronic structures of these oxo complexes are currently ongoing. Additionally, both the atom transfer and redox properties of these oxo compounds are being explored to determine their potential future applications.

Acknowledgment. S.C.B. would like to thank the Alexander von Humboldt Foundation for a postdoctoral fellowship. This research was supported by grants from the U.S. Department of Energy (DOE grant DE-FG02-O4ER 15537), DFG, and SFB 583. Dr. C. Hauser (FAU) is gratefully acknowledged for her assistance with preparation of this manuscript.

Supporting Information Available: Experimental procedures, crystallographic data, and computational details. This material is available free of charge via the Internet at <http://pubs.acs.org>.

JA804263W